

# Sparse-view computed tomography image reconstruction via a combination of $L_1$ and $SL_0$ regularization

Hongliang Qi, Zijia Chen, Jingyu Guo and Linghong Zhou\*  
*Institute of Medical Instruments, School of Biomedical Engineering, Southern Medical University, 510515, Guangzhou, China*

**Abstract.** Low-dose computed tomography reconstruction is an important issue in the medical imaging domain. Sparse-view has been widely studied as a potential strategy. Compressed sensing (CS) method has shown great potential to reconstruct high-quality CT images from sparse-view projection data. Nonetheless, low-contrast structures tend to be blurred by the total variation (TV,  $L_1$ -norm of the gradient image) regularization. Moreover, TV will produce blocky effects on smooth and edge regions. To overcome this limitation, this study has proposed an iterative image reconstruction algorithm by combining  $L_1$  regularization and smoothed  $L_0$  ( $SL_0$ ) regularization.  $SL_0$  is a smooth approximation of  $L_0$  norm and can solve the problem of  $L_0$  norm being sensitive to noise. To evaluate the proposed method, both qualitative and quantitative studies were conducted on a digital Shepp-Logan phantom and a real head phantom. Experimental comparative results have indicated that the proposed  $L_1/SL_0$ -POCS algorithm can effectively suppress noise and artifacts, as well as preserve more structural information compared to other existing methods.

Keywords: Sparse-view reconstruction, smoothed  $L_0$  regularization,  $L_1$  regularization, total variation

## 1. Introduction

X-ray computed tomography (CT) has been extensively applied in medical diagnosis over the past few decades. However, excessive X-ray radiation delivered to the patients during clinical examinations may increase a risk of cancer [1-3]. Therefore, it is necessary to minimize the radiation risk while maintaining acceptable image quality in clinical practice. Decreasing milliampere-seconds (low-mAs) and under-sampling the needed projections (sparse-view) are being studied as important strategies to reduce CT imaging dose [4-7]. If the projection data is collected through low-mAs modality, the sinograms will contain much noise and CT image reconstructed by filtered back-projection (FBP) [8] will be degraded. For sparse-view image reconstruction, conspicuous streaking artifacts exist in CT images since the FBP algorithms need the number of projections to theoretically satisfy the Nyquist sampling rule [9]. Therefore, it is important to develop new algorithms in order to

---

\* Address for correspondence: Linghong Zhou, Institute of Medical Instruments, School of Biomedical Engineering, Southern Medical University, 510515, Guangzhou, China. Tel.: +86 20 61648291; Fax: +86 20 62789510; E-mail: smart@smu.edu.cn.

obtain acceptable clinical images from low-mAs or few-view projections. Sparse-view reconstruction will be the focus in this work.

Mathematically, CT image reconstruction from sparse views is an ill-posed problem. In recent years, CS theory [10, 11] has been studied in CT reconstruction. Specifically, total variation (TV) regularization [12], which is defined as  $L_1$ -norm of gradient image (GI), has demonstrated great potential in CT reconstruction with limited number of x-ray projections [13, 14]. Although TV-based methods have achieved efficient results, one shortcoming of TV method is to uniformly regularize the image gradient ignoring the structural information. This disadvantage to some extent may lead to smoothed edges and blocky effects. Many efforts have been made to address this issue [15-20]. Chang, et al. proposed a few-view reweighed sparsity hunting (FRESH) method for CT image reconstruction [15]. Tian, et al. proposed an edge preserving TV (EPTV) model [16]. This model can preserve edges by bringing different weights in TV according to edges and homogeneous areas in an image. Different from the EPTV model, an adaptive-weighted TV model for low-dose sparse-view CT image reconstruction was established by Liu, et al. based on the consideration of the anisotropic edge property as an image [17]. Zhang, et al. used a high-order norm coupled within TV to overcome the disadvantages of traditional TV minimization [18]. Theoretically, a regularization, which is close to  $L_0$  norm which denotes the number of nonzero signal elements, could obtain higher-quality CT images in CT reconstruction. Chen, et al. used the sparser  $L_{1/2}$  regularization operator [19] ( $L_{1/2}$ -norm of GI) to replace the traditional  $L_1$  regularization and combined the Split Bregman method to do the reconstruction. Although  $L_0$  regularization is the sparsest and most ideal regularization norm,  $L_0$ -norm minimization problems have been recognized to be NP-hard, and it is difficult to solve equations. Sun, et al. has proposed an iterative algorithm (named as IHT-POCS (POCS, projection onto convex sets)) based on the  $L_0$ -norm of GI [20]. Such an approach using a pseudo-inverse transform of GI and adapting the IHT algorithm aims to address the challenges introduced by the  $L_0$ -norm of GI. Nonetheless, the sparse level  $S$  in IHT-POCS can only be roughly estimated. Moreover,  $L_0$  regularization is susceptible to noise interference.

In this paper, an iterative algorithm for sparse-view CT image reconstruction based on a combined  $L_1$  and smoothed  $L_0$  regularization was proposed. The reconstruction method is called  $L1/SL_0$ -POCS in this work. Specifically, in  $L1/SL_0$ -POCS, three steps are involved: 1) POCS reconstruction; 2)  $TV_{L_1}$  ( $L_1$ -norm of GI) minimization; 3)  $TV_{SL_0}$  ( $SL_0$ -norm of GI) minimization. To assess the proposed  $L1/SL_0$ -POCS algorithm, quantitative and qualitative studies were conducted on a digital Shepp-Logan phantom and a real head phantom.

## 2. Method

### 2.1. CT reconstruction with TV minimization from sparse-view data

Mathematical model [21] of CT image reconstruction can be expressed in a linear equation.

$$y = Au \quad (1)$$

where  $y = (y_1, y_2, \dots, y_M)^T$  represents the obtained projection data after log-transformation at different projection directions,  $u = (u_1, u_2, \dots, u_N)^T$  is the image vector to be estimated and ' $T$ ' is the transpose operator.  $A$  is a projection matrix with the size of  $M \times N$ . Numerically, element  $a_{ij}$  in  $A$  can be described as the contribution of the pixel  $j$  to the x-ray  $i$ , and can be calculated by ray tracing

algorithm [22]. However, Eq. (1) is an ill-posed problem when the measured data is sparse, and there exist infinitely many solutions to Eq. (1).

To solve this problem, Sidky *et al.* presented an iterative scheme [13, 14] through POCS with TV minimization for few-view reconstruction problem by solving the following constrained optimization problem:

$$\min \|u\|_{TV} \quad \text{subject to} \quad |y - Au| \leq \varepsilon, u \geq 0 \tag{2}$$

where  $\varepsilon$  is a parameter which describes the inconsistency between the measured projection data and the estimated data. The expression of TV, i.e.  $\|u\|_{TV}$ , is defined as:

$$\|u\|_{TV} = \|\nabla u\|_1 = \sum_{s,t} \sqrt{(u_{s,t} - u_{s-1,t})^2 + (u_{s,t} - u_{s,t-1})^2} \tag{3}$$

where  $s$  and  $t$  are the indices of the location of the discrete image, and  $\nabla u$  is the gradient image. Eq. (2) can be effectively solved by TV-POCS [13] and ASD-POCS [14] which consist of POCS and gradient descent in each iteration.

Although the TV model has been successfully applied to reconstruct high-quality CT images, edges with low-contrast tend to be over-smoothed. In addition, TV suffers from the notorious blocky effect which limits the clinical practice of TV.

### 2.2. Smoothed $L_0$ regularization ( $SL_0$ )

In CS theory,  $L_0$  norm is the most ideal regularization norm, but it is difficult to solve equations with  $L_0$  norm which is sensitive to noise in CT reconstruction, so  $L_0$  norm is usually replaced by  $L_1$  norm. It should be noted that conventional TV is the  $L_1$  norm of gradient image (GI). Theoretically, applying a regularization norm closer to  $L_0$  norm will help reconstruct higher-quality CT images. Therefore, replacing  $L_0$  norm with a norm much closer to  $L_0$  will yield desirable images.

In fact, the problem of using  $L_0$  norm is due to the fact that the  $L_0$  norm of a vector is a discontinuous function of that vector. Mohimani, *et al.* has presented smoothed  $L_0$  norm ( $SL_0$ ) to approximate this discontinuous function by a suitable continuous (smoothed) one [23].

Define

$$f_\sigma(t) = \exp(-t^2 / 2\sigma^2) \tag{4}$$

Then

$$\lim_{\sigma \rightarrow 0} f_\sigma(t) = \begin{cases} 1 & t = 0 \\ 0 & t \neq 0 \end{cases} \tag{5}$$

Therefore,

$$\|s\|_{L_0} \approx N - \sum_{j=1}^N \lim_{\sigma \rightarrow 0} f_\sigma(s_j) = \|s\|_{SL_0} \tag{6}$$

where  $\sigma$  is a parameter used to specify trade-off between accuracy and smoothness.  $N$  is the number of elements in vector  $s$ .

In literature [23], the smoothed  $L_0$  norm ( $SL_0$ ) provides a smooth measure of sparsity, and the problem of high sensitivity of  $L_0$  norm to low-level of noise is solved. It has been applied in compressible sensing MRI imaging.  $SL_0$  is able to recover or reconstruct image well in the presence of low-level of noise. However, if the image to be processed contains a higher level of noise,  $SL_0$  cannot balance the relationship between noise and reconstruction precision, which degrades the image and produces apparent noise points.

### 2.3. The proposed CT image reconstruction method ( $L1/SL0$ -POCS)

The goals of the proposed combination of  $L_1$  and  $SL_0$  is, firstly to use  $L_1$  regularization to remove most of the noise in noisy images, and then to apply  $SL_0$  regularization to remove the rest of the noise in the images regularized by  $L_1$  and preserve the detailed structure information. The proposed method makes full use of respective advantages from  $L_1$  and  $SL_0$  to regularize noisy images to a maximum extent. In this study, CT reconstruction problem can be expressed as

$$\min\{\|\nabla u\|_{L_1} + \|\nabla u\|_{SL_0}\} = \min\{\|u\|_{TV} + \|u\|_{TVSL_0}\} \quad \text{subject to} \quad |y - Au| \leq \epsilon, u \geq 0 \tag{7}$$

To solve the optimization problem of Eq. (7), three iterative steps are involved: 1) POCS reconstruction; 2)  $TV_{L_1}$  minimization; 3)  $TV_{SL_0}$  minimization. In POCS of step 1, SART algorithm [24, 25] and positivity constraint are used to update an estimated image.

$TV$  minimization and  $TV_{SL_0}$  minimization can be implemented using the gradient descent based method. The image  $TV$  ( $\|u\|_{TV}$ ) is defined as shown in Eq. (3) and the image  $TV_{SL_0}$  can be expressed as

$$\|u\|_{TVSL_0} = \|\nabla u\|_{SL_0} = N - \sum_{s,t} f_\sigma(\sqrt{(u_{s,t} - u_{s-1,t})^2 + (u_{s,t} - u_{s,t-1})^2}) \tag{8}$$

where  $f_\sigma(t) = \exp(-t^2/2\sigma^2)$ ,  $\sigma$  is a parameter for small positive smoothing, and  $N$  is the number of pixels in a two-dimensional (2D) image.

Accordingly, the derivatives of  $\|u\|_{TV}$  and  $\|u\|_{TVSL_0}$  are respectively:

$$\nabla_u \|u\|_{TV} = \frac{\partial \|u\|_{TV}}{\partial u_{s,t}} \approx \frac{(u_{s,t} - u_{s-1,t}) + (u_{s,t} - u_{s,t-1})}{\nabla u_{s,t} + \rho} - \frac{u_{s+1,t} - u_{s,t}}{\nabla u_{s+1,t} + \rho} - \frac{u_{s,t+1} - u_{s,t}}{\nabla u_{s,t+1} + \rho} \tag{9}$$

$$\begin{aligned} \nabla_u \|u\|_{TVSL_0} = \frac{\partial \|u\|_{TVSL_0}}{\partial u_{s,t}} \approx & \exp(-\nabla u_{s,t}^2 / 2\sigma^2) \nabla u_{s,t} / \sigma^2 \frac{(u_{s,t} - u_{s-1,t}) + (u_{s,t} - u_{s,t-1})}{\nabla u_{s,t} + \rho} \\ & - \exp(-\nabla u_{s+1,t}^2 / 2\sigma^2) \nabla u_{s+1,t} / \sigma^2 \frac{u_{s+1,t} - u_{s,t}}{\nabla u_{s+1,t} + \rho} \\ & - \exp(-\nabla u_{s,t+1}^2 / 2\sigma^2) \nabla u_{s,t+1} / \sigma^2 \frac{u_{s,t+1} - u_{s,t}}{\nabla u_{s,t+1} + \rho} \end{aligned} \tag{10}$$

where  $\rho$  is the number of small positive to keep the denominator not equal to zero.

In summary, the formulas for  $TV$  and  $TVSL_0$  minimization are shown respectively as follow:

Table 1

Implementation steps of L1/SL0-POCS reconstruction
Algorithm of L1/SL0-POCS
Initialization: Give $A, y, K, Q1, Q2$ and $w$ . Main loop for $k=1,2,\dots,K$
1. Reconstruction by SART
$u_j^{k+1} = u_j^k + \frac{w}{A_{+,j}} \sum_{i=1}^M \frac{A_{i,j}}{A_{i,+}} (y_i - \sum_{j=1}^N A_{i,j} u_j^k)$
2. Positivity constraint
$u^{k+1,1} = \max(u^{k+1}, 0)$
3. TV minimization loop
$u^{k+1,q+1} = u^{k+1,q} - \alpha_1 \cdot \Delta u \cdot \frac{\nabla \ u^{k+1,q}\ _{TV}}{\ \nabla \ u^{k+1,q}\ _{TV}\ }$
for $q=1,2,\dots,Q1$
4. $u^{k+1,Q1,1} = u^{k+1,Q1}$
5. TVSL0 minimization loop
$u^{k+1,Q1,q+1} = u^{k+1,Q1,q} - \alpha_2 \cdot \Delta u \cdot \frac{\nabla \ u^{k+1,Q1,q}\ _{TVSL0}}{\ \nabla \ u^{k+1,Q1,q}\ _{TVSL0}\ }$
for $q=1,2,\dots,Q2$
6. $u^{k+2} = u^{k+1,Q1,Q2}$
7. Return to Step 1 until the stopping criterion is satisfied.

$$u^{p+1} = u^p - \alpha_1 \cdot \Delta u \cdot \frac{\nabla \|u^p\|_{TV}}{\|\nabla \|u^p\|_{TV}\|} \quad u^{q+1} = u^q - \alpha_2 \cdot \Delta u \cdot \frac{\nabla \|u^q\|_{TVSL0}}{\|\nabla \|u^q\|_{TVSL0}\|} \tag{11}$$

where  $\alpha_1, \alpha_2$  are the step sizes and  $p, q$  are the iteration indexes.  $\Delta u$  is the difference between the reconstructed images at the  $k$ th and  $(k+1)$  iterations. The image reconstructed by SART at the  $k$ th iteration is used as an input for TV minimization, and the image after TV minimization is employed for  $TV_{SL0}$  minimization. The implementation steps of L1/SL0-POCS reconstruction are shown in Table 1.

#### 2.4. Parameter selection for proposed L1/SL0-POCS

It is important to determine the optimal parameters for L1/SL0-POCS. For  $w$  in SART, it is often set to be 1.0 in SART based on reconstruction methods [19, 24, 25]. For  $\alpha_j$  and  $Q1$  in TV minimization, they are set to be 0.2 and 5 respectively, which is done similarly in TV-POCS method [13, 14]. Through extensive experiments, we found parameters  $\alpha_2$  and  $Q2$ , which are also set to be 0.2 and 5 respectively, could achieve a good compromise between noise suppression and computational efficiency.

For iteration cycle  $K$ , in our experiments, it is sufficient to produce good and acceptable results when  $K$  equals to 100. More iteration number could not make the reconstructed image improve apparently. Therefore, we believe the reconstruction will be stopped mandatorily if the iteration index  $k$  reaches 100. This type of stopping criterion is often used in CT reconstructions.

For smooth parameter  $\sigma$  in  $\|u\|_{TVSL_0}$ , it is related to standard deviation of the image noise, but the noise distribution during reconstruction is non-stationary and unknown. Therefore, it is also empirically set ( $\sigma=10^{-3}$ ) in this study.

The parameters in our  $L_1/SL_0$ -POCS are set empirically by using setups from similar methods and through extensive experiments by visual inspection and quantitative measures, which is time-consuming. The main goal of this work is to demonstrate the effectiveness of the proposed regularization. How to select optimal parameters effectively is a significant research in the future.

### 3. Experiments

#### 3.1. Numerical simulation

In this section, we conduct a numerical experiment to study FBP, SART, TV-POCS and  $L_1/SL_0$ -POCS algorithms. Shepp-Logan phantom with size of  $256 \times 256$  is used. Without losing generality, a fan beam imaging geometry is chosen to acquire the projection data. The distance between X-ray source and rotation axis is 40 cm and the distance between detector and rotation axis is 40 cm. The image is  $25.6 \times 25.6$  cm<sup>2</sup>. The detector with a length of 61.44 cm is a line array consisting of 512 elements. X-ray projections are simulated using ray-driven method [24]. A total of 30 projections are equally distributed over a 360 degree range. The tests in this paper are implemented by MATLAB programming language on a PC with Intel(R) Core(TM) 2 Quad CPU 2.50 GHz and 3.25 GB RAM.

The reconstructed images are shown in Figure 1. It can be observed that serious streak artifacts exist in the CT image reconstructed by FBP algorithm. Obviously, there are also serious streak artifacts and noticeable smoothing effect in SART image. The TV-POCS reconstruction is shown in Figure 1(c) and the blocky artifacts in the homogeneous regions are obvious and the edges are partially over-smoothed. Figure 1(e) shows the proposed  $L_1/SL_0$ -POCS reconstruction. It can be noticed that the  $L_1/SL_0$ -POCS algorithm performs great potential in suppressing artifacts and preserving edges information by using  $SL_0$  regularization.

Figure 2 shows the zoomed-in views of two ROIs corresponding to Figure 1, respectively. It can be found that image reconstructed by  $L_1/SL_0$ -POCS algorithm is comparable with the ground true image and achieves better gains in terms of noise suppression and edges preservation.

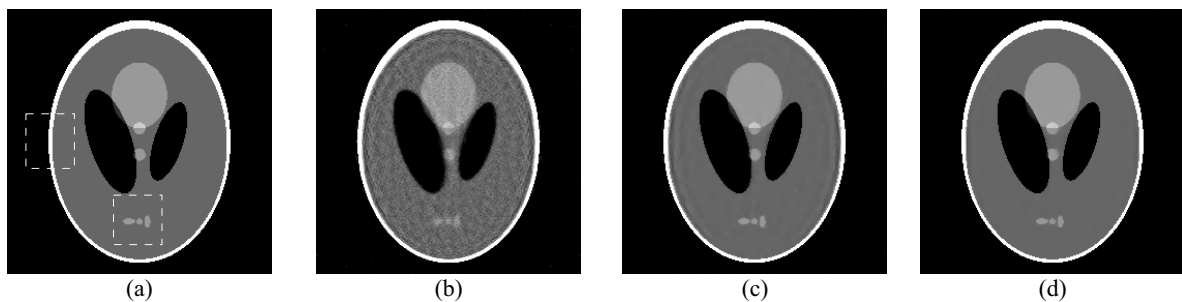


Fig. 1. Reconstructed images of Shepp-Logan phantom from 30 projections. (b)–(d) correspond to the reconstructions using SART, TV-POCS, and  $L_1/SL_0$ -POCS, respectively. (a) is the original phantom.

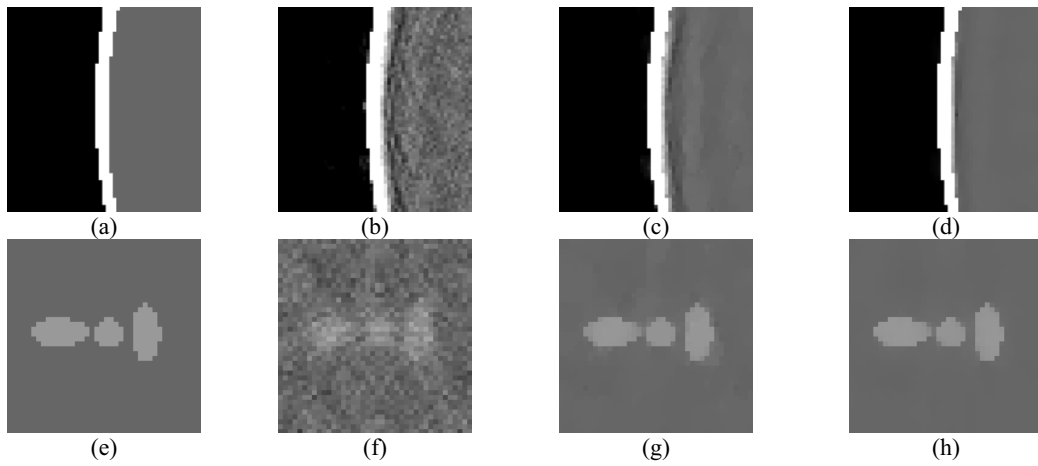


Fig. 2. Zoomed-in views of two ROIs shown in Figure 1. (b)–(d) correspond to the reconstructions using SART, TV-POCS, and L1/SL0-POCS, respectively and (a) is the original phantom. (f)–(h) correspond to the reconstructions using SART, TV-POCS, and L1/SL0-POCS, respectively and (e) is the original phantom.

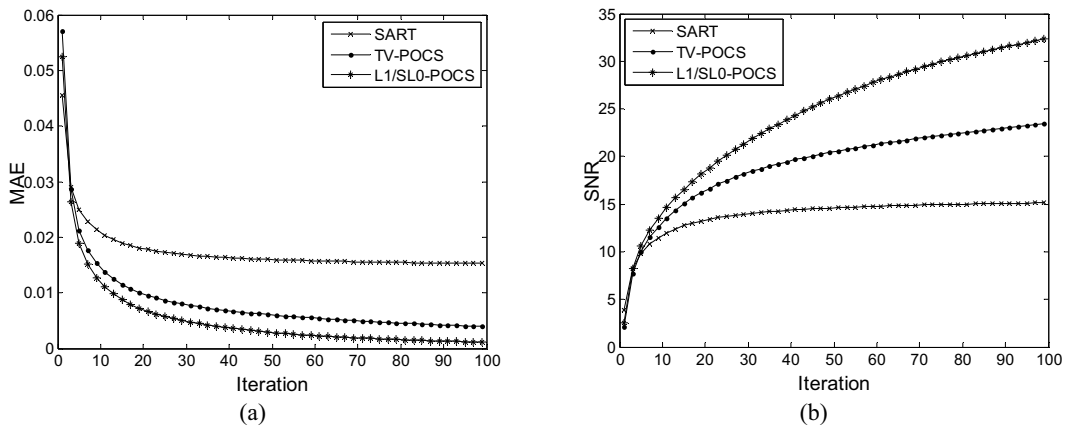


Fig. 3. The MAE (a) and SNR (b) curves of reconstructed images with different reconstruction algorithms at 30 projection angles and different iteration numbers, and the iteration numbers range from 1 to 100.

To evaluate the reconstructed images, the mean absolute error (MAE) and signal to noise ratio (SNR) are used. As shown in Figure 3, our proposed L1/SL0-POCS algorithm achieves lower MAE and higher SNR compared with the other two methods, which means that L1/SL0-POCS can reconstruct high-quality images in less iteration numbers.

### 3.2. Real data experiment

#### 3.2.1. Pseudo-real data

In this section, previously reconstructed CT volume is used to study the proposed method. The CT volume ( $512 \times 512 \times 25$ ) is scanned with tube voltage of 130 KeV and reconstructed. The pixel size and a slice size are 0.29 mm and 2.0 mm respectively. A slice is used and projected forward respectively into 40 projections in 360 degree by using Siddon’s ray-driven algorithm. The proposed method will be made comparison with SART and TV-POCS.

The reconstructed images from the 40-view data by using SART, TV-POCS, and L1/SL0-POCS algorithms are displayed in Figure 4. Visual inspection of reconstructions suggests that the TV-POCS and L1/SL0-POCS algorithms can effectively suppress streak artifacts and noise observed in SART images. It could be found that the images reconstructed by L1/SL0-POCS preserve more structural edged details than images using TV-POCS. Moreover, the blocky effect caused by TV is suppressed efficiently in Figure 4(d), compared to Figure 4(c).

### 3.2.2. Real data

To evaluate the performance of proposed algorithm for X-ray CT, reconstruction study with real CT projection data is also performed. Single circle scan and fan beam imaging geometry are used to obtain the projections in our developed laboratory CT scanner. A head phantom as scanned object is used. 360 projections are evenly captured over a 360 degree range. Image reconstructed by FBP using 360 projections is shown in Figure 5(d) as true reference image.

The projections are down-sampled to 90 views, about one-fourth of the full views. The reconstructions from 90 projection views are shown in Figure 5. Reconstructed images are of  $512 \times 512$  pixels. These reconstructed images demonstrate that the proposed method can significantly improve image quality. Teeth are clearly preserved and observed while homogeneous regions are smoothed well.

## 4. Conclusion

In this paper, a L1/SL0-POCS method for low-dose CT reconstruction from few-view projection

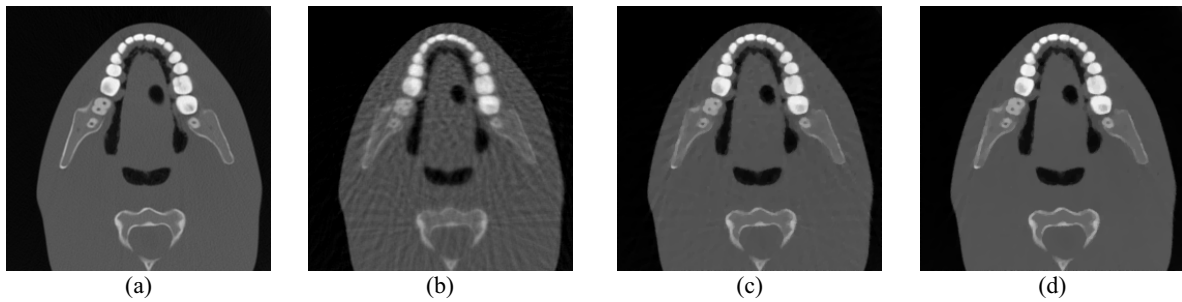


Fig. 4. Reconstructed images of head phantom from 40 projections. (b)–(d) correspond to the reconstructions using SART, TV-POCS, and L1/SL0-POCS, respectively, and (a) is the first original image.

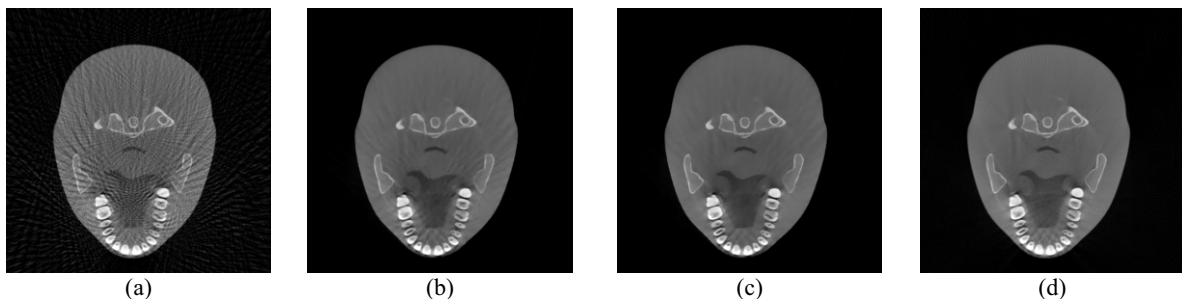


Fig. 5. Reconstructed images of a head phantom. (a) to (c) correspond to the reconstructions using FBP, TV-POCS and L1/SL0-POCS from 90 projections. (d) corresponds to the reconstruction using FBP from 360 projections.

data is proposed. The main contribution of the method is to minimize a combined  $L_1$  and smoothed  $L_0$  ( $SL_0$ ) regularization instead of traditional TV regularization. The performance of the proposed method is compared to SART and TV-POCS methods on Shepp-logan phantom and a real head phantom. Experimental results show that the proposed  $L_1/SL_0$ -POCS algorithm is able to achieve better performance compared with other existing methods in the MAE, SNR and edge information preservation. One issue that should be paid attention to is the computation cost. From the numerical scheme of the proposed method, it can be clearly seen that the computational cost of  $L_1/SL_0$ -POCS is on the same level of TV-POCS. In one iteration of TV-POCS and  $L_1/SL_0$ -POCS methods, the computation time are 40.48s and 44.33s respectively for Shepp-Logan phantom, which is possible to use some acceleration strategies to overcome their drawbacks of time-consuming computation.

Many clinical conditions are not considered in our present study due to the limitation of the experimental conditions. Future work will focus more on verifying the proposed algorithm in real clinical projections. Moreover, the presented algorithm can be easily extended to cone beam CT (CBCT) geometry due to its iterative-correction property. Meanwhile, low-dose CBCT reconstruction by the proposed GPU-acceleration method will also be studied in CBCT system in the future research.

## References

- [1] E.J. Hall and D.J. Brenner, Cancer risks from diagnostic radiology, *The British Journal of Radiology* **81** (2008), 362–378.
- [2] A.B. de Gonzalez, M. Mahesh, K.P. Kim, M. Bhargavan, R. Lewis, F. Mettler and C. Land, Projected cancer risks from computed tomographic scans performed in the united states in 2007, *Archives of Internal Medicine* **169** (2009), 2071–2077.
- [3] R. Smith-Bindman, J. Lipson, R. Marcus, K.P. Kim, M. Mahesh, R. Gould, A.B. de Gonzalez and D.L. Miglioretti, Radiation dose associated with common computed tomography examinations and the associated lifetime attributable risk of cancer, *Archives of Internal Medicine* **169** (2009), 2078–2086.
- [4] M.K. Kalra, C. Wittram, M.M. Maher, A. Sharma, G.B. Avinash, K. Karau, T.L. Halpern, S. Saini and J.A. Shepard, Can noise reduction filters improve low-radiation-dose chest CT images? Pilot study 1, *Radiology* **228** (2003), 257–264.
- [5] M.K. Kalra, M.M. Maher, T.L. Toth, L.M. Hamberg, M.A. Blake, J.A. Shepard and S. Saini, Strategies for CT radiation dose optimization, *Radiology* **230** (2004), 619–628.
- [6] C.H. McCollough, M.R. Bruesewitz and J.M. Kofler, CT dose reduction and dose management tools: Overview of available options, *Radiographics* **26** (2006), 503–512.
- [7] L.F. Yu, X. Liu, S. Leng, J.M. Kofler, J.C. Ramirez-Giraldo, M.L. Qu, J. Christner, J.G. Fletcher and C.H. McCollough, Radiation dose reduction in computed tomography: Techniques and future perspective, *Imaging in Medicine* **1** (2009), 65–84.
- [8] G.T. Gullberg, The reconstruction of fan-beam data by filtering the back-projection, *Computer Graphics and Image Processing* **10** (1979), 30–47.
- [9] A.J. Jerri, The Shannon sampling theorem—Its various extensions and applications: A tutorial review, *Proceedings of the IEEE* **65** (1977), 1565–1596.
- [10] D.L. Donoho, Compressed sensing, *IEEE Transactions on Information Theory* **52** (2006), 1289–1306.
- [11] E.J. Candes, J. Romberg and T. Tao, Robust uncertainty principles: Exact signal reconstruction from highly incomplete frequency information, *IEEE Transactions on Information Theory* **52** (2006), 489–509.
- [12] L.I. Rudin, S. Osher and E. Fatemi, Nonlinear total variation based noise removal algorithms, *Physica D: Nonlinear Phenomena* **60** (1992), 259–268.
- [13] E.Y. Sidky, C. Kao and X. Pan, Accurate image reconstruction from few-views and limited-angle data in divergent-beam CT, *Journal of X-ray Science and Technology* **14** (2006), 119–139.
- [14] E.Y. Sidky and X. Pan, Image reconstruction in circular cone-beam computed tomography by constrained, total-variation minimization, *Physics in Medicine and Biology* **53** (2008), 4777–4807.
- [15] M. Chang, L. Li, Z.Q. Chen, Y. Xiao, L. Zhang and G. Wang, A few-view reweighted sparsity hunting (FRESH) method for CT image reconstruction, *Journal of X-ray Science and Technology* **21** (2013), 161–176.
- [16] Z. Tian, X. Jia, K. Yuan, T. Pan and S.B. Jiang, Low-dose CT reconstruction via edge-preserving total variation

- regularization, *Physics in Medicine and Biology* **56** (2011), 5949–5967.
- [17] Y. Liu, J. Ma, Y. Fan and Z. Liang, Adaptive-weighted total variation minimization for sparse data toward low-dose x-ray computed tomography image reconstruction, *Physics in Medicine and Biology* **57**(2012), 7923–7956.
  - [18] Y. Zhang, W. Zhang, H. Chen, M.L. Yang and J.L. Zhou, Few-view image reconstruction combining total variation and a high-order norm, *International Journal of Imaging Systems and Technology* **23** (2013), 249–255.
  - [19] M. Chen, D. Mi, P. He, L. Deng and B. Wei, A CT reconstruction algorithm based on  $L_{1/2}$  regularization, *Computational and Mathematical Methods in Medicine* **2014** (2014), 862910.
  - [20] Y.L. Sun and J.X. Tao, Image reconstruction from few views by  $\ell_0$ -norm optimization, *Chinese Physics B* **23** (2014), 078703.
  - [21] G. Wang and M. Jiang, Ordered-subset simultaneous algebraic reconstruction techniques (OS-SART), *Journal of X-Ray Science and Technology* **12** (2004), 169–177.
  - [22] R.L. Siddon, Fast calculation of the exact radiological path for a three-dimensional CT array, *Medical Physics* **12** (1985), 252–255.
  - [23] G.H. Mohimani, M. Babaie-Zadeh and C. Jutten, A fast approach for overcomplete sparse decomposition based on smoothed  $L_0$  norm, *IEEE Transactions on Signal Processing* **57** (2008), 289–301.
  - [24] A.H. Andersen and A.C. Kak, Simultaneous algebraic reconstruction technique (SART): A superior implementation of the art algorithm, *Ultrason Imaging* **6** (1984), 81–94.
  - [25] M. Jiang and G. Wang, Convergence of the simultaneous algebraic reconstruction technique (SART), *IEEE Transactions on Image Processing* **12** (2003), 957–961.